SAMPLING BELOW THE NYQUIST RATE IN INTERFEROMETRIC FLUORESCENCE MICROSCOPY WITH MULTI-WAVELENGTH MEASUREMENTS TO REMOVE ALIASING

Brynmor J. Davis, W. Clem Karl, Bennett B. Goldberg, Anna K. Swan, M. Selim Ünlü

Department of Electrical and Computer Engineering
Boston University
8 St. Mary's Street
Boston, MA 02215 USA

ABSTRACT

A multi-wavelength 3D fluorescence microscope, with transfer functions varying significantly with wavelength, is proposed. This microscope measures multiple wavelengths concurrently and scans through the object at a rate significantly below the Nyquist criterion, which gives a reduced image acquisition time. The sub-Nyquist sampling produces a set of images contaminated by aliasing. Due to the differing transfer functions, the aliasing effects are different in each image. This allows the aliasing operator to be inverted and a single unaliased image to be constructed. This is an application of the generalized sampling expansion first introduced by Papoulis. The instrument is demonstrated through simulation and shown to produce images of a similar quality to those that would be expected from a Nyquist-rate instrument.

1. INTRODUCTION

Fluorescence microscopy is an important tool in biology due, in part, to its ability to image live specimens and to utilize high specificity fluorescent markers. The utility of fluorescence microscopy has been increased by modern three-dimensional instruments that have achieved resolution on a sub-cellular scale. Prominent among these modern instruments are systems that rely on interferometric techniques [1, 2].

In order to construct a three-dimensional image, a fluorescence microscope must scan through the object in multiple spatial dimensions. To avoid aliasing, the spatial scanning rate must satisfy the Nyquist criterion [3]. This requirement results in significant image acquisition time. The method proposed here reduces this time by allowing a sub-Nyquist spatial scanning rate. The reduced image acquisition time is particularly important in applications that involve imaging an evolving object.

Typically, only light of one wavelength is collected in a microscope. Here many wavelengths will be collected simultaneously, with differing optical interference properties, to produce multiple images. This means that light that would typically be discarded is now collected and processed usefully, and that the object is being observed through multiple channels. This diversity in observation is what allows the reduction in scanning rate.

For a 1D system it has been shown that the use of M channels allows sampling at a rate of $1/M$ times the Nyquist frequency [4]. This result does impose certain conditions on the allowable impulse responses in order to assure well-posedness and does not address noise issues. Ill-posed and noisy problems are considered in [5] and [6]. For the interferometric fluorescence microscopy application, the problem will also be noisy and ill-posed, as beyond a given spatial-frequency support the instrument passes no information.

By considering systems of dimension two and higher, sampling efficiencies can be found by considering the spectral support of the signal to be sampled and the spatial sampling pattern [7]. This approach has also been incorporated into multi-channel systems [8] but will not be considered here. For simplicity a regular, rectangular sampling grid will be considered, however more general systems and conditions are the subject of on-going research [9, 10].

In the following section, the theory of sampling and image reconstruction for multiple channels is reviewed in the context of this application. Instrument design and description are then covered, followed by some illustrative examples. Lastly, conclusions are drawn.
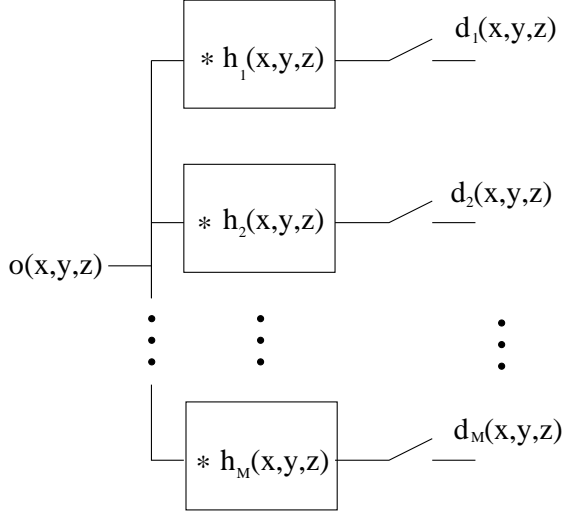
Fig. 1. Block diagram of the observation model. Note that the sets of data collected $d_m(x,y,z)$ are sampled at identical rates and will, in general, be below the Nyquist rate.

2. MULTI-CHANNEL SAMPLING AND RECONSTRUCTION

A generic observation model of the proposed system is given in Fig. 1. An object is passed through M linear, shift-invariant observation channels and the resulting data sets are sampled. The sampling to be considered here will be below the Nyquist rate and identical in each channel.

If sampling is performed on a three-dimensional rectangular grid, the collected data can be easily related to the object and the system responses in the Fourier domain [3].

$$D_m\left(\overline{f}\right) = \frac{1}{T_x T_y T_z} \sum_{\overline{f}_s \in A} H_m\left(\overline{f} - \overline{f}_s\right) O\left(\overline{f} - \overline{f}_s\right) \quad (1)$$

Here capitalization indicates a Fourier domain representation of the lowercase function. The term $\overline{f}$ is the spatial-frequency vector (f_x, f_y, f_z), T_x, T_y and T_z are the sampling periods and the set A gives the spectral replication offsets.

$$\begin{aligned}
A =\; & \left(\ldots, \frac{-2}{T_x}, \frac{-1}{T_x}, 0, \frac{1}{T_x}, \frac{2}{T_x}, \ldots\right) \\
& \times \left(\ldots, \frac{-2}{T_y}, \frac{-1}{T_y}, 0, \frac{1}{T_y}, \frac{2}{T_y}, \ldots\right) \\
& \times \left(\ldots, \frac{-2}{T_z}, \frac{-1}{T_z}, 0, \frac{1}{T_z}, \frac{2}{T_z}, \ldots\right) \quad (2)
\end{aligned}$$

If the Nyquist criterion is met, then only one term in the sum of Eqn. 1 will be non-zero for any value of $\overline{f}$. This means that the continuous signal can easily be recovered by using a band-pass filter, which performs interpolation in the spatial domain. If the Nyquist criterion is not met then more than one term (say N terms) will contribute at each value of $\overline{f}$ in the sum. For the multi-channel system, this gives the following observation model.

$$\begin{bmatrix} D_1\left(\overline{f}_1\right) \\ D_2\left(\overline{f}_1\right) \\ \vdots \\ D_M\left(\overline{f}_1\right) \end{bmatrix} = \mathbf{H}\left(\overline{f}_1\right) \begin{bmatrix} O\left(\overline{f}_1\right) \\ O\left(\overline{f}_2\right) \\ \vdots \\ O\left(\overline{f}_N\right) \end{bmatrix} \quad (3)$$

Where $\overline{f}_2, \cdots, \overline{f}_N$ are the frequencies that alias into $\overline{f}_1$ and $\mathbf{H}\left(\overline{f}_1\right)$ is the aliasing operator.

$$\mathbf{H}\left(\overline{f}_1\right) =$$
$$\begin{bmatrix} H_1\left(\overline{f}_1\right) & H_1\left(\overline{f}_2\right) & \cdots & H_1\left(\overline{f}_N\right) \\ H_2\left(\overline{f}_1\right) & H_2\left(\overline{f}_2\right) & \cdots & H_2\left(\overline{f}_N\right) \\ \vdots & \vdots & \ddots & \vdots \\ H_M\left(\overline{f}_1\right) & H_M\left(\overline{f}_2\right) & \cdots & H_M\left(\overline{f}_N\right) \end{bmatrix} \quad (4)$$

If the aliasing operator $\mathbf{H}\left(\overline{f}_1\right)$ can be inverted at $\overline{f}_1$, then the spatial frequencies $\overline{f}_1, \overline{f}_2, \cdots, \overline{f}_N$ can be reconstructed from the M sub-Nyquist/aliased images collected. Note that if the Nyquist criterion is met then $\mathbf{H}\left(\overline{f}_1\right)$ becomes a column vector.

The required invertibility of $\mathbf{H}\left(\overline{f}_1\right)$ gives some obvious conditions on the system, e.g. the matrix cannot have more columns than rows so the under-sampling factor N cannot be greater than the number of measurements collected. In the presence of noise, invertibility alone is not enough to ensure a good reconstruction. Issues such as solution existence and noise amplification [11] become important. For these reasons it is desirable to have a well conditioned aliasing operator. How the microscope can be designed to ensure this is considered in the next section.

The reconstruction approach taken in this preliminary work will be to do a simple truncated singular value decomposition (TSVD) inversion [12] of the aliasing matrix at each value of $\overline{f}_1$. That is, components of the object that would be too noisy in the reconstruction are discarded. This retention threshold constitutes the regularization parameter for this reconstruction method.

If $\mathbf{G}\left(\overline{f}_1\right)$ is this TSVD inverse, then $\mathbf{GH}\left(\overline{f}_1\right)$ represents the overall effect of the aliasing and the reconstruction. A way of measuring the purity of the recovered frequency component $\hat{O}\left(\overline{f}_n\right)$ is to measure the contribution to it from the true component $O\left(\overline{f}_n\right)$. Here $\overline{f}_n \in \left(\overline{f}_1, \overline{f}_2, \cdots, \overline{f}_N\right)$.

$$\rho(\overline{f}_n) = \frac{|\left(\mathbf{GH}\left(\overline{f}_1\right)\right)_{nn}|}{\sqrt{\sum_{m=1}^{M} |\left(\mathbf{GH}\left(\overline{f}_1\right)\right)_{nm}|^2}} \quad (5)$$

Here the double subscripts denote a particular entry in the matrix. If the matrix $\mathbf{GH}\left(\overline{f}_1\right)$ is the identity (ideal case), then $\rho\left(\overline{f}_n\right) = 1 \; \forall \; n$.
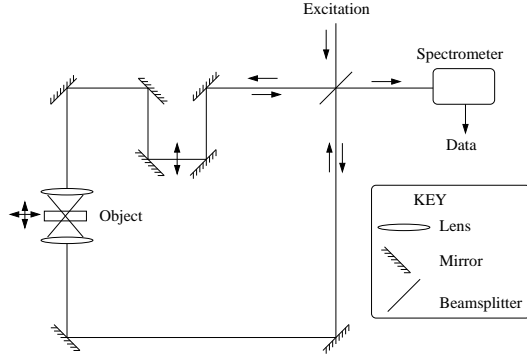
Fig. 2. Schematic of the proposed microscopy system. Important features include interferometric excitation and/or detection, an adjustable path delay between the two arms of the system and multi-wavelength detection.

3. MULTI-WAVELENGTH INTERFEROMETRIC MICROSCOPY

In fluorescence microscopy the object is first stained with a fluorescent dye. This dye is then excited by light at a specific wavelength which causes the fluorophores to emit over a set of longer wavelengths. This emitted light is then collected and used to form an image of the fluorophore density. Interferometric fluorescence microscopy systems such as 4Pi [1] and I^{5}M [2] excite and/or collect from both sides of the object and combine the two beams coherently at the detector. This results in interference and a higher achievable resolution.

Here multiple emission wavelengths will be collected at the same time to give many observation channels. As mentioned in Section 2, it is desirable to have a system that produces a well-conditioned aliasing operator. It is for that reason that this method is applied to interferometric systems. Introducing a path delay between the two excitation/collection arms causes the interference properties to change with the wavelength collected — i.e. a path length that produces constructive optical interference at a given wavelength will produce destructive interference at a nearby wavelength (see [13] for a discussion of optical interference). This will result in significantly differing channel properties at each wavelength and thus the potential to create a well-conditioned aliasing operator (if all the channels are similar then the rows of $\mathbf{H}\left(\overline{f}_1\right)$ will be similar and this will result in a poorly conditioned matrix). A diagram of the proposed system is shown in Fig. 2. This system is a generalization of that proposed in [14].

The effects of changing the interference properties are primarily visible in the depth/axial dimension of the system, which will be denoted by z. The point spread functions of the channels remain relatively unchanged perpendicular to this axis. For this reason, sub-Nyquist sampling will only
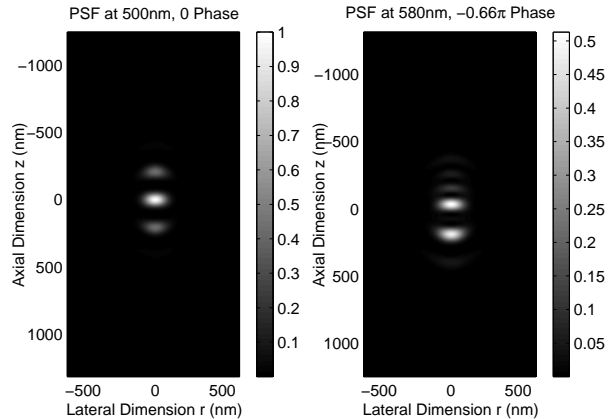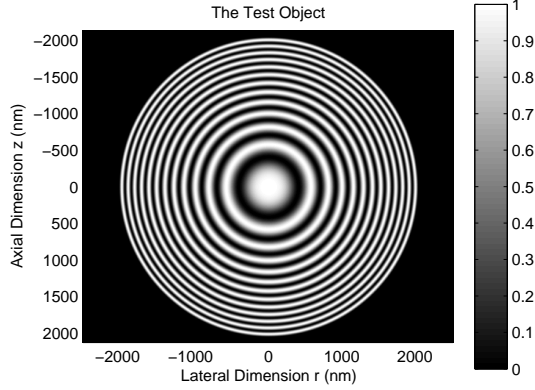

Fig. 3. Point spread functions for the 4Pi microscope when the detection is at a wavelength of 500nm and 580nm. The delay between the two arms is set to give zero phase offset (constructive interference) at 500nm and -0.66π phase offset at 580nm.

be carried out in the z direction. This means aliasing will only occur along the axial axis and an axial sampling rate of between $1/(N-1)$ and $1/N$ times the Nyquist rate will result in N columns in the aliasing operator $\mathbf{H}\left(\overline{f}_1\right)$.

Finally, it is worth making a comment on the noise in fluorescence microscopy systems. The data collected obeys (to a good approximation) a Poisson noise model. This means that a longer collection time at each scan position will give a higher photon count and thus better noise characteristics. However, the overall goal in this paper is to reduce image acquisition time. Since the system collects wavelengths that would otherwise be discarded in a single-wavelength-detection system, the photon count is not reduced. In other words, it takes the same amount of time with either system to scan a given position to achieve a certain noise level but the multi-wavelength system needs to scan less positions and thus gives a better image acquisition time.

4. RESULTS

A modified 4Pi-Type-C [1] microscope was considered for these examples. The modifications were the addition of multi-wavelength detection and a path delay between the detection arms. The excitation wavelength was taken to be 488nm and the collected emissions were limited to the range 500-580nm. The numerical aperture of the lenses used was 1.35 and the excitation light was taken to be circularly polarized. These parameters are the same as those used in [15] and the same method for calculating the point spread functions was employed. That is, the method is based on the vectorial optics result from [16].
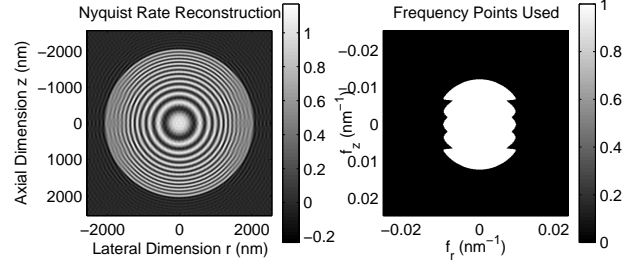
Fig. 4. The test object to be used to validate the reconstruction method.

Fig. 5. Reconstruction of the test object from a single Nyquist-rate channel (left). The Fourier components that are used to create the reconstruction are shown on the right — a value of 1 indicates the component was used.

Fig. 6. Reconstruction of the object from two channels sampled at half the Nyquist rate (left). The purity measure $\rho(\overline{f})$ is shown on the right.

Two example point spread functions are shown in Fig. 3. It can be seen that the instrument produces significantly different point spread functions at different wavelengths. Note that although the point spread functions are three dimensional, the microscope geometry assures that they will be cylindrically symmetric around the axial axis. For this reason it is only necessary to display an axial (z) vs lateral ($\sqrt{x^2 + y^2}$) image to describe the point spread function.

This cylindrical symmetry property will be retained for display purposes throughout these examples. In order to do this, a cylindrically symmetric test object will be chosen. Fig. 4 shows this test object. It is a collection of concentric sinusoidal oscillations with decreasing period. The minimum period corresponds to the maximum spatial frequency passed by the instrument.

For the sake of comparison, a reconstruction will be produced from a single channel scanned above the Nyquist rate. This is shown in Fig. 5 where the single channel is at a 500nm detection wavelength and has zero phase delay. Note that the reconstruction has been interpolated (using zero padding in the Fourier domain) to have the same 10nm × 10nm grid as used in the original test object (Fig. 4). The object is reconstructed well except for at the high lateral spatial frequencies where the oscillations fall outside the instrument passband. The mean square difference between the reconstruction and the original object is 0.0051. Note that the regularization parameter is set to allow a comparatively large passband — this corresponds to relatively low noise levels. Also, the reconstruction is not windowed in the Fourier domain so ringing artifacts can be expected.

The first sub-Nyquist example considered will be when two wavelengths are collected and the axial scanning is carried out at half the Nyquist rate. The two channels used correspond to the point spread functions shown in Fig. 3. The reconstruction and the purity measure (Eqn. 5) are shown in Fig. 6. It can be seen that the usable frequency domain
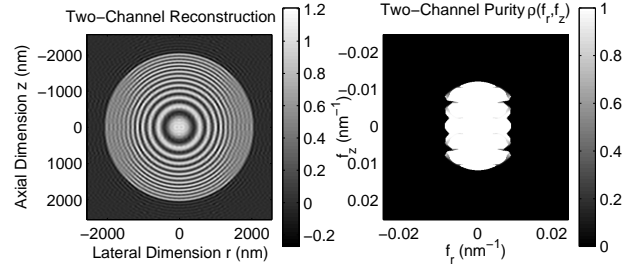
components are similar to the single-channel, Nyquist-rate example (the same regularization parameter was used). Frequency domain zero-padding was again used to put the reconstructions on a common grid. The mean square error in this case is 0.0076.

The next example uses five wavelengths (500nm, 527nm, 540nm, 553nm, 580nm) with a delay that gives phase shifts of 0, 0.5π, 0.66π, -0.5π and -0.66π respectively. Each of these channels will be sampled at one quarter of the Nyquist rate. The resulting reconstruction and purity measure are shown in Fig. 7. For this low sampling rate the loss of usable Fourier domain components is noticeable. The reconstruction quality is also noticeably lower. This is reflected in the mean square error which is 0.0095 for this example.

As would be expected, the results presented here have shown that the technique proposed becomes less effective as higher gains in image acquisition time are attempted. Although not shown here, it is also true that performance degrades (in comparison to the Nyquist-rate single channel) as noise is increased. An increased noise requires stronger regularization and the aliasing cannot be inverted as cleanly.
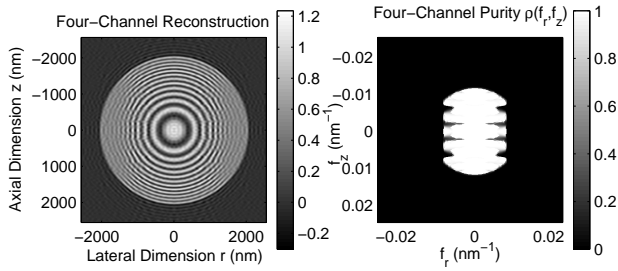
Fig. 7. Reconstruction of the object from four channels sampled at one quarter the Nyquist rate (left). The purity measure $\rho(\overline{f})$ is shown on the right.

5. CONCLUSIONS

Multi-channel sampling and reconstruction theory has been applied to an interferometric fluorescence microscopy application. The multi-channel approach allows a sub-Nyquist spatial sampling rate which gives a reduction in image acquisition time — an important consideration in high resolution microscopy. The time improvement demonstrated here is on the order of a factor of 2 to 4. This method relies on a dedicated post-processing operation and an instrument with significantly differing channels.

The theory was demonstrated through simulation on a modified 4Pi fluorescence microscope. While these simulations showed encouraging results, it should be noted that the microscope was not optimized to work in a multi-channel setting. There are many modifications that could be made to the system that may give properties more suited to multi-channel operation. Of particular interest would be introducing pupil filters to the lenses to allow point spread function engineering (e.g. [17]). Design issues such as this are an area of future research.

6. REFERENCES

[1] S. Hell and E. H. K. Stelzer, "Properties of a 4Pi confocal fluorescence microscope," *J. Opt. Soc. Am. A*, vol. 12, pp. 2159–2166, Dec. 1992.

[2] M. G. L. Gustafsson, D. A. Agard, and J. W. Sedat, "I⁵M: 3D widefield light microscopy with better than 100nm axial resolution," *J. Microsc.*, vol. 195, pp. 10–16, July 1999.

[3] A. V. Oppenheim and R. W. Schafer, *Discrete-Time Signal Processing*, Pearson Education, second edition, 1998.

[4] A. Papoulis, "Generalized sampling expansion," *IEEE Trans. Circuits Syst.*, vol. 24, pp. 652–654, Nov. 1977.

[5] K. F. Cheung and R. J. Marks II, "Ill-posed sampling theorems," *IEEE Trans. Circuits Syst.*, vol. 32, pp. 481–484, May 1985.

[6] N. P. Galatsanos, A. K. Katsaggelos, R. T. Chin, and A. D. Hillery, "Least squares restoration of multichannel images," *IEEE Trans. Signal Processing*, vol. 39, pp. 2222–2236, Oct. 1991.

[7] K. F. Cheung and R. J. Marks II, "Imaging sampling below the Nyquist density without aliasing," *J. Opt. Soc. Am. A*, vol. 7, pp. 92–105, Jan. 1990.

[8] K. F. Cheung, "A multidimensional extension of Papoulis' generalized sampling expansion with the application in minimum density sampling," in *Advanced Topics in Shannon Sampling and Interpolation Theory*, R. J. Marks II, Ed., chapter 3, pp. 85–119. Springer-Verlag, 1993.

[9] G. Harikumar and Y. Bresler, "Exact image deconvolution from multiple FIR blurs," *IEEE Trans. Image Processing*, vol. 8, pp. 846–862, June 1999.

[10] R. Venkataramani and Y. Bresler, "Sampling theorems for uniform and periodic nonuniform MIMO sampling of multiband signals," *IEEE Trans. Signal Processing*, vol. 51, pp. 3152–3163, Dec. 2003.

[11] W. C. Karl, "Regularization in image restoration and reconstruction," in *Handbook of Image and Video Processing*, A. Bovik, Ed., chapter 3, pp. 141–161. Academic Press, 2000.

[12] P. C. Hansen, *Rank-Deficient and Discrete Ill-Posed Problems*, SIAM, 1998.

[13] E. Hecht, *Optics*, Addison Wesley, 4th edition, 2001.

[14] A. K. Swan, L. A. Moiseev, C. R. Cantor, B. Davis, S. B. Ippolito, W. C. Karl, B. B. Goldberg, and M. S. Ünlü, "Toward nanometer-scale resolution in fluorescence microscopy using spectral self-interference," *IEEE J. Select. Topics Quantum Electron.*, vol. 9, pp. 294–300, Mar./Apr. 2003.

[15] M. Nagorni and S. Hell, "Coherent use of opposing lenses for axial resolution increase. I. Comparitive study of concepts," *J. Opt. Soc. Am. A*, vol. 18, pp. 36–48, Jan. 2001.

[16] B. Richards and E. Wolf, "Electromagnetic diffraction in optical systems. II. Structure of the image field in an aplanatic system," *Proc. Roy. Soc. A*, vol. 253, pp. 358–379, Dec. 1959.

[17] C. J. R. Sheppard and Z. S. Hegedus, "Axial behavior of pupil-plane filter," *J. Opt. Soc. Am. A*, vol. 5, pp. 643–647, May 1988.